Science World Journal Vol. 20(No 3) 2025 https://dx.doi.org/10.4314/swj.v20i3.5
www.scienceworldjournal.org
ISSN: 1597-6343 (Online), ISSN: 2756-391X (Print)
Published by Faculty of Science, Kaduna State University

Full Length Research Article

ELECTRONIC, MECHANICAL, VIBRATIONAL, OPTICAL AND THERMOELECTRIC PROPERTIES OF $RbIO_3$: A DENSITY FUNCTIONAL THEORY (DFT) APPROACH

*Morka J.C., Nwachuku D.N., Osuho P.O. and Kanayo S.

Department of Physics, University of Delta, Agbor

*Corresponding Author Email Address: john.morka@unidel.edu.ng

ABSTRACT
Spin-polarized density functional theory (SP-DFT) is a theoretical framework that incorporates spin polarization into DFT calculations, allowing for the investigation of magnetic systems and phenomena where spin-dependent effects play a crucial role. The aim of employing spin-polarized density functional theory (SP-DFT) is to accurately describe and predict the magnetic and electronic structures of systems with the goal of gaining insights into their spin-dependent behavior and properties. This study used the Quantum Espresso package to investigate the structural, electronic, mechanical, lattice dynamic, and optical properties of cubic perovskite $RbIO_3$. Spin-polarized density functional theory (SP-DFT) based ab-initio calculations were conducted to investigate the structural, mechanical, electronic, lattice dynamic, and optical properties of cubic perovskite $RbIO_3$. The analysis of the lattice parameter-energy relationship indicated that the compound is neither ferromagnetic nor non-magnetic. Mechanical stability criteria for cubic structures confirmed that the material is stable and ductile. Electronic band structure calculations showed semiconducting behaviour. This band gap transformation suggests potential applications in optoelectronic, photovoltaic, and photochemical devices. However, phonon dispersion curves indicated dynamic instability due to the presence of negative frequencies. Key optical properties, including refractive index n(ω), absorption coefficient α(ω), reflectivity R(ω), electron energy-loss spectrum L(ω), extinction coefficient k(ω), and optical conductivity, were examined. The results indicate that cubic $RbIO_3$ exhibits optical activity in the visible to ultraviolet regions. The bulk modulus of the material is very hard

Keywords: Density Functional Theory (DFT), Optical Properties, Optoelectronic applications, Thermodynamic Properties.

INTRODUCTION

The perovskite structure is one of the most common crystal structures found in solid-state inorganic chemistry. The ideal perovskite structure has an ABX_3 composition, featuring a 3D network of corner-sharing BX_6 octahedra. The A-site cation resides in the 12-coordinate cavities created by the BX_3 framework, with 12 neighbouring anions at equal distance. This structure can accommodate a vast range of metallic ions from the periodic table, as well as various anions. While most perovskites are oxides or fluorides, heavier halides are also known to form this structure (Lufaso & Woodward, 2001).

Among ternary oxides, perovskites are the most common and have been extensively studied using first-principles calculations due to their remarkable properties. Cubic perovskites, which crystallize in the space group Pm-3m (#221), represent the most stable and symmetrical form of this structure. Over the past few decades, perovskites and their derivatives have attracted significant research interest due to their diverse and technologically important properties, including ferromagnetism (Khandy & Gupta, 2017), superconductivity (Schneemeyer et al., 1987), spin polarization (El Rhazouani et al., 2016), colossal magnetoresistance (Raveau et al., 1998), and thermoelectricity (Reshak, 2016).

For instance, Bouadjemi et al. (2015) suggested that $NdMnO_3$ could be a promising material for spintronic and optoelectronic applications based on their theoretical analysis of its structural, magnetic, and optical properties. Similarly, $BaTiO_3$ has been explored for use in electro-optic devices and ceramic capacitors (Pithan et al., 2005; Tian et al., 2009; Tsurumi et al., 2002). Ferroelectric perovskites are particularly valuable in microwave applications, such as phase shifters, varactors, tunable oscillators, and detectors, making them ideal for electrically tunable devices (Jindal et al., 2018).

Recent studies have examined the magnetic and thermoelectric properties of cubic tantalum-based perovskites, $XTaO_3$ (X = Rb, Fr) (Hussain et al., 2021). These materials exhibit notable band gaps—$RbTaO_3$ has an indirect gap of 1.12 eV, while $FrTaO_3$ shows a direct gap of 1.08 eV. Sarwan et al. (2020) used the FP-LAPW method to analyze $RbTaO_3$'s structural, elastic, and electronic properties, confirming its stability in the perovskite phase and revealing its brittle nature. Meanwhile, DFT studies on $NdInO_3$ suggest its potential for UV-optical devices due to its strong UV absorption (Butt et al., 2020).

Further investigations using DFT-GGA calculations on $Ba_{1-x}Ca_xTiO_3$ and $Ba_{1-x}Sr_xTiO_3$ (x = 0.4, 0.6) revealed an indirect transition at the M-point (Tahiri et al., 2018). The relationship between microstructure and dielectric/mechanical losses in $BaxSr_{1-x}TiO_3$ was also explored, showing that composition and grain size influence phase transitions (Cheng et al., 2002). Additionally, pressure-dependent studies (0–75 GPa) on $RbTaO_3$ demonstrated a transition from an indirect to a direct band gap, with significant effects on its electronic, optical, and thermoelectric behavior (Hassan et al., 2021).

However, existing studies on $RbIO_3$ lack detailed insights into its structural and lattice dynamic stability under pressure, as well as its magnetic properties. To address these gaps, this study employs the Quantum ESPRESSO package to investigate the structural, electronic, mechanical, lattice dynamic, and optical properties of cubic perovskite $RbIO_3$.

Computational detail

The study employed the QUANTUM ESPRESSO (QE) code, utilizing a first-principles approach based on SP-DFT (Giannozzi et al., 2009), to examine the material's properties. The calculations

Science World Journal Vol. 20(No 3) 2025 https://dx.doi.org/10.4314/swj.v20i3.5
www.scienceworldjournal.org
ISSN: 1597-6343 (Online), ISSN: 2756-391X (Print)
Published by Faculty of Science, Kaduna State University

incorporated the Projected Augmented Wave (PAW) pseudopotential (Perdew et al., 1996) and the Generalized Gradient Approximation (GGA) with the Perdew-Burke-Ernzerhof (PBE) functional (Perdew et al., 1997) to model electron exchange interactions, bonding, and magnetic behavior. Prior to the main computations, convergence tests were performed to determine the optimal kinetic energy cutoff and k-point mesh sampling. The calculations used a Monkhorst-Pack grid of 8×8×8, a kinetic energy cutoff of 110 Ry, and a convergence threshold of 10^{-8} eV/atom for total energy. The valence electron configurations were set as Rb ($5s^1$), I ($4d^{10}\ 5s^2\ 5p^5$), and O ($2s^2\ 2p^4$). The cubic structure of $RbIO_3$ (Figure 1) adopts the Pm-3m (221) space group, with Rb, I, and O atoms occupying the Wyckoff positions 1a (0,0,0), 1b (½,½,½), and 3c (½,½,0), respectively.

RESULTS AND DISCUSSION

Structural and Mechanical Properties.

The structural and mechanical properties of $RbIO_3$ perovskite in its ground state were investigated. The cubic perovskite structure was geometrically optimized in both non-magnetic (NM) and ferromagnetic (FM) states by minimizing the total energy with respect to variations in lattice parameters. Through self-consistent calculations, the equilibrium lattice constant (a), bulk modulus (B), and its pressure derivative (B') were determined and listed in Table 1. The energy-lattice curve (Figure 2) indicates that the compound exhibits neither ferromagnetic nor non-magnetic behaviour.

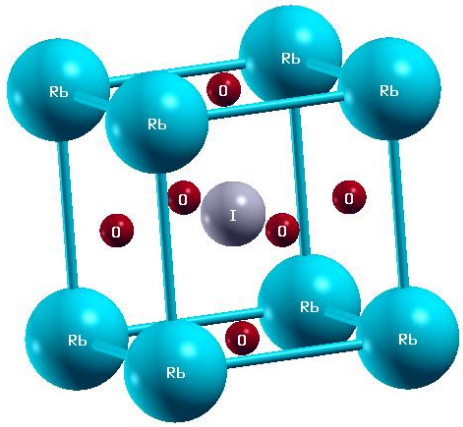

Figure 1. The crystal structure of $RbIO_3$

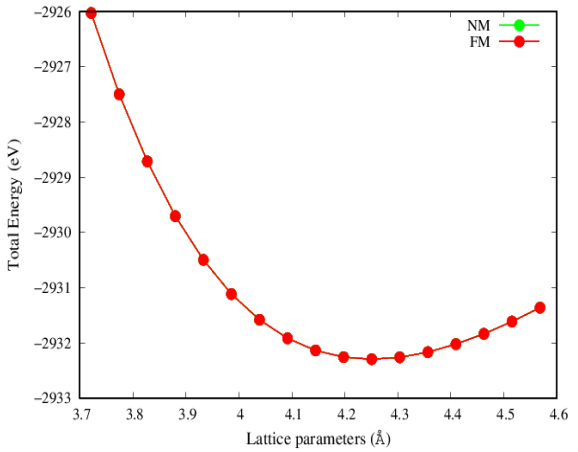

Figure 2. The total energies per unit cell as a function of lattice constants for the Ferromagnetic (FM) and Non-magnetic (NM) states of the alloy

To assess geometric stability, the Goldschmidt tolerance factor (t) was calculated using the formula [21]:

$$t = \frac{(r_A + r_O)}{\sqrt{2}(r_B + r_O)} \quad (1)$$

where r_A, r_B, and r_O represent the ionic radii of the A-site cation, B-site cation, and oxygen anion, respectively. A stable perovskite typically has a tolerance factor between 0.8 and 1.04. Additionally, the octahedral factor ($\mu = r_B/r_O$) was evaluated, with stable structures falling within $0.414 < \mu < 0.732$. For $RbIO_3$, t = 1.0429 and μ = 2.3333, confirming its stability.

Mechanical stability in cubic systems depends on elastic constants, with the criteria: $C_{11} + 2C_{12} > 0$, $C_{11} - C_{12} > 0$, $C_{44} > 0$, and $C_{11} > 0$ (Wu et al., 2007; Sin'ko & Smirnow, 2002). The compound meets these conditions, indicating elastic stability. To determine ductility or brittleness, key parameters include Poisson's ratio (υ), Pugh's ratio (B/G), and Cauchy pressure (C_{12} - C_{44}) (Iyorzor et al., 2018; Bakare et al., 2017; Pugh, 1954). A B/G ratio above 1.75 suggests ductility, as observed in $RbIO_3$ (Table 1). Poisson's ratio (0–0.5) reflects bonding nature, while a positive Cauchy pressure further confirms ductility, and a positive CP is often associated with increased toughness and resistance to crack propagation (Boucetta, 2014).

Electronic Properties.

The electronic band structure of cubic perovskite $RbIO_3$ exhibits semiconducting behavior, with the Fermi level positioned at the top of the valence band. At 0 GPa, the valence band maximum and the conduction band minimum are located at the M-point, resulting in a direct band gap of 0.596 eV, as illustrated in Figures 3-4.

Science World Journal Vol. 20(No 3) 2025 https://dx.doi.org/10.4314/swj.v20i3.5
www.scienceworldjournal.org
ISSN: 1597-6343 (Online), ISSN: 2756-391X (Print)
Published by Faculty of Science, Kaduna State University

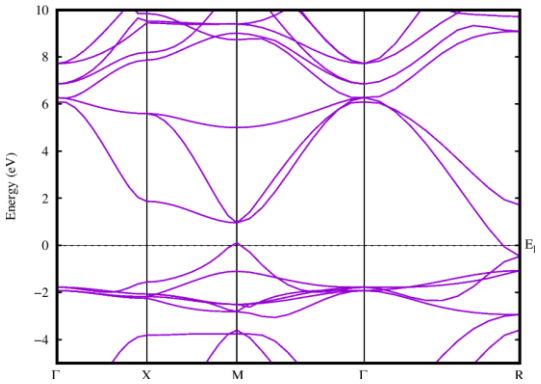

Figure 3. Electronic band structures of $RbIO_3$

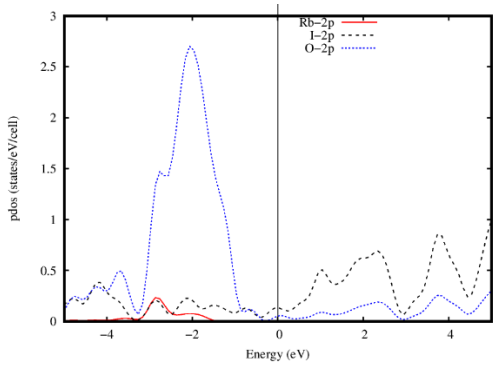

Figure 4. The PDOS of $RbIO_3$

The partial density of states (PDOS) for $RbIO_3$ reveals the orbital contributions to bonding and electronic structure. The purpose of the PDOS plot is to shed light on the type of bonding between the orbitals and the effect of individual orbitals on the DOS. At 0GPa, within the conduction band, the major contribution originated from the I-2p orbital and little from the O-2p orbital. Their effect is far from the Fermi energy level. Similarly, in the valence band, the three orbitals made their individual contributions, with O-2p orbital having the highest contribution and the least from Rb-3p orbital.

Table 1. The Mechanical/Structural properties of cubic perovskite $RbIO_3$

Properties	Results
a (Å)	8.0326
B (GPa)	107.1
C_{11}	199.9
C_{12}	63.6
C_{44}	57.8
E (GPa)	153.2
G (GPa)	60.7
B/G	1.8
n	0.3

Vibrational properties

To investigate the vibrational characteristics of the $RbIO_3$ compound, we calculated its phonon spectrum. The computations were performed using the Thermo_pw package, which relies on Quantum ESPRESSO routines as its computational engine for determining material properties. The phonon dispersion curves along the high-symmetry directions Γ–X–M–Γ–R–X are presented in Figure 5. A key observation was the presence of imaginary (negative) frequencies in the Brillouin zone, revealing the compound's dynamic instability.

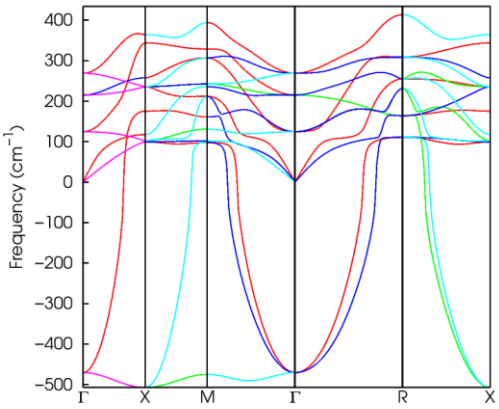

Figure 5: Phonon dispersion curves along symmetry directions of $RbIO_3$ at pressure 0GPa

Optical properties

The optical properties of the $RbIO_3$ compound spanning an energy range of 0–18.4 eV, are illustrated in Figures 6(a-g). These properties were derived from the complex dielectric function, $\varepsilon(\omega) = \varepsilon_1(\omega) + i\varepsilon_2(\omega)$, which characterizes the interaction of incident radiation with the material. The dielectric function represents the system's linear response to external electromagnetic fields.

The imaginary part of the dielectric function, $\varepsilon_1(\omega)$, was determined using momentum matrix elements between occupied and unoccupied wave functions, while the real part, $\varepsilon_1(\omega)$, was obtained via the Kramers-Kronig transformation (Hu et al., 2007). At zero frequency, the static dielectric constant $\varepsilon_1(\omega)$ was found to be 5.62 (Figure 6(a)). In the $\varepsilon_2(\omega)$ spectra, the maximum peaks occur at 5.38 eV (Figure 6(b)).

Key optical parameters including the refractive index (n(ω)), absorption coefficient (α(ω)), reflectivity (R(ω)), electron energy-loss spectrum (L(ω)). Key properties, including extinction coefficient (kw) and optical conductivity, were calculated based on the dielectric function. The absorption coefficient, crucial for evaluating solar energy conversion efficiency, indicates the extent to which a material absorbs light at specific energies. It represents the attenuation of light intensity as it passes through the material and is defined as the absorption cross-section per unit volume.

For $RbIO_3$, the absorption coefficient occurred at 2.78 eV. The highest peaks are observed at 30.79(ω), as shown in Figure 6(c). The compound exhibits strong absorption across a broad range (5–16 eV) in the low-energy region.

Reflectivity (R(ω)), depicted in Figure 6(d), reaches maxima of 32.7% at 5.9 eV, indicating that 67.3% of incident UV radiation is absorbed.

The refractive index (n(ω)) at zero frequency yields static values of 2.37 (Figure 6e). The electron energy-loss function (L(ω)), which reveals electron interactions such as interband transitions, plasmon excitations, and phonon effects (Azzouz et al., 2019), displays sharp peaks at 6.31 eV, 14.29 eV, and 17.99 eV for 0 GPa (Figure 6(f). The minimal energy loss in the infrared, visible, and

Science World Journal Vol. 20(No 3) 2025 https://dx.doi.org/10.4314/swj.v20i3.5
www.scienceworldjournal.org
ISSN: 1597-6343 (Online), ISSN: 2756-391X (Print)
Published by Faculty of Science, Kaduna State University

lower UV regions suggests promising optical applications for $RbIO_3$.

Finally, the extinction coefficient (k(ω)), representing electromagnetic wave attenuation, increases from 0.22 to 0.82 in the visible range, peaking at 1.69 (5.75 eV) in the UV region (Figure 6(g)).

Conclusion

We have investigated and presented the structural, electronic, mechanical, lattice dynamics and optical properties of the Cubic Perovskite RbIO3 using First Principles calculations as implemented in the QUANTUM ESPRESSO code. Firstly, the tolerance factor 't' and the octahydral factor 'μ' which are empirical measures that links the perovskite $RbIO_3$ chemical composition to its stability were investigated. The results for 't' and 'μ' satisfy the requirements, hence the compound is considered to be structurally stable. Mechanically, from the values of the B/G ratio and cauchy relation the material is found to be ductile. Also, it is elastically stable against deformation from the elastic constants criteria. And the results of the bulk modulus reveal that the material is very hard. It was found that the electronic band structure of the compound is purely semiconductor, and has a direct band gap of 0.596 eV. the $RbIO_3$ compound is a good contender for optoelectronic, photovoltaic and photochemistry devices applications (Azzouz et al., 2019). The lattice dynamics of the compound was investigated with the use of Thermo_pw code and imaginary (negative) frequencies in the Brillouin zone was observed. This feature reveals that it is dynamically unstable. The various optical quantities are also calculated and discussed. The optical band gaps from the absorption coefficient spectrum are found to be close to the energy band gap of the material.

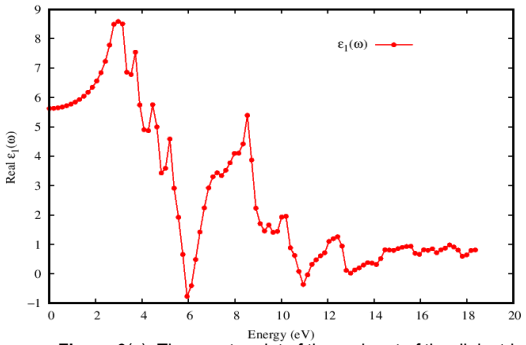

Figure 6(a): The spectra plot of the real part of the dielectric function $\varepsilon_1(\omega)$ between occupied and unoccupied wave function at zero frequency

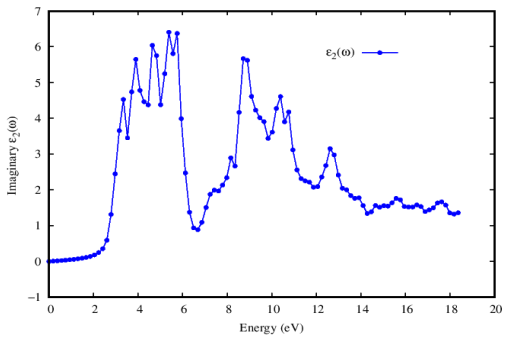

Figure 6(b): The spectra plot of the imaginary part of the dielectric function $\varepsilon_2(\omega)$ between occupied and unoccupied wave function at zero frequency

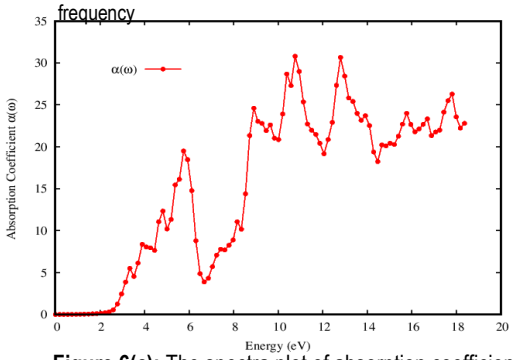

Figure 6(c): The spectra plot of absorption coefficient of $RbIO_3$ against photon energy

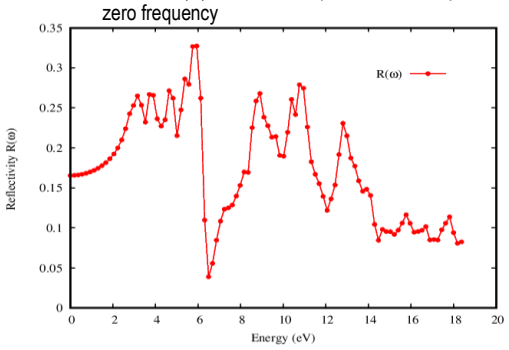

Figure 6(d): The spectra plot of reflectivity of $RbIO_3$ against photon energy

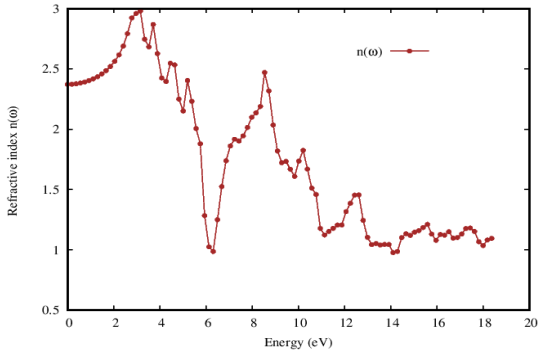

Figure 6(e): The spectra plot of refractive index of $RbIO_3$ against photon energy

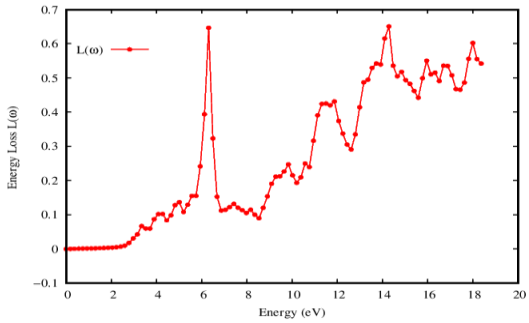

Figure 6(f): The spectra plot of energy loss of $RbIO_3$ against photon energy

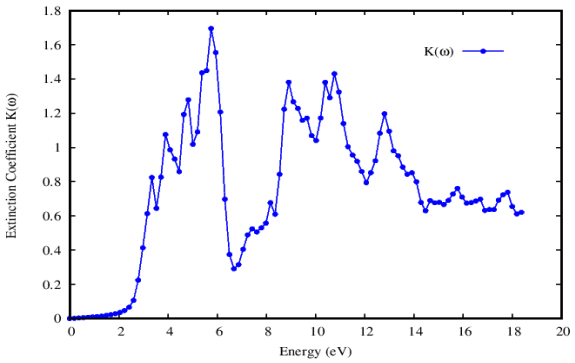

Figure 6(g): The spectra plot of extinction coefficient of $RbIO_3$ against photon energy

REFERENCES

Bakare F. O., Babalola M. I. and Iyorzor B. E. (2017). Materials Research Express, 4(11), 116502.

Bouadjemi, B., Bentata, S., Abbad, A., & Benstaali, W. (2015). Ab-initio study of optoelectronic and magnetic properties of the orthorhombic NdMnO3 perovskite. Solid State Communications, 207, 9-15.

Boucetta S. (2014). Journal of Magnesium and Alloy 2, 59.

Butt, M. K., Yaseen, M., Ghaffar, A., & Zahid, M. (2020). First principle insight into the structural, optoelectronic, half metallic, and mechanical properties of cubic perovskite NdInO3. Arabian Journal for Science and Engineering, 45(6), 4967-4974.

Cheng, B. L., Su, B., Holmes, J. E., Button, T. W., Gabbay, M., & Fantozzi, G. (2002). Dielectric and mechanical losses in (Ba, Sr) TiO3 systems. Journal of electroceramics, 9(1), 17-23.

El Rhazouani, O., Zarhri, Z., Benyoussef, A., & El Kenz, A. (2016). Magnetic properties of the fully spin-polarized Sr2CrOsO6 double perovskite: A Monte Carlo simulation. Physics Letters A, 380(13), 1241-1246.

Giannozzi, P., Baroni, S., Bonini, N., Calandra, M., Car, R., Cavazzoni, C., Ceresoli, D., Chiarotti, G.L., Cococcioni, M., Dabo, I. and Dal Corso, A., (2009). Journal of physics: Condensed matter, 21(39), p.395502.

Hassan, M., Liaqat, M., & Mahmood, Q. (2021). Pressure dependence of electronic, optical and thermoelectric properties of RbTaO3 perovskite. Applied Physics A, 127(4), 1-8.

Hu, J. M., Huang, S. P., Xie, Z., Hu, H., & Cheng, W. D. (2007). First-principles study of the elastic and optical properties of the pseudocubic Si3As4, Ge3As4 and Sn3As4. Journal of Physics: Condensed Matter, 19(49), 496215.

Hussain, M. I., Khalil, R. A., Hussain, F., & Rana, A. M. (2021). DFT-based insight into the magnetic and thermoelectric characteristics of XTaO3 (X= Rb, Fr) ternary perovskite oxides for optoelectronic applications. International Journal of Energy Research, 45(2), 2753-2765.

Ilyas, A., Khan, S. A., Liaqat, K., & Usman, T. (2021). Investigation of the structural, electronic, magnetic, and optical properties of CsXO3 (X= Ge, Sn, Pb) perovskites: A first-principles calculations. Optik, 244, 167536.

Iyorzor B. E., Babalola M. I., Adetunji B. I. and Bakare F. O. (2018). Effect of Tellurium concentration on the sructural, electronic and mechanical properties of Beryllium Sulphide: DFT approach. Materials Research Express, 5(5), 056517.

Jindal, S., Vasishth, A., Devi, S., & Anand, G. (2018). A review on tungsten bronze ferroelectric ceramics as electrically tunable devices. Integrated Ferroelectrics, 186(1), 1-9.

Khandy, S. A., & Gupta, D. C. (2017). Structural, elastic and magneto-electronic properties of half-metallic BaNpO3 perovskite. Materials Chemistry and Physics, 198, 380-385.

Lufaso, M. W., and Woodward, P. M. (2001). Prediction of the crystal structures of perovskites using the software program SPuDS. Acta Crystallographica Section B: Structural Science, 57(6), 725-738.

Perdew JP, Burke K, Ernzerhof M. (1996). Generalized gradient approximation made simple. Phys. Rev. Lett. 77, 3865–3868.

Perdew JP, Burke K, Ernzerhof M. (1997). Generalized gradient approximation made simple. Phys. Rev. Lett. 78, 1396.

Pithan, C., Hennings, D., & Waser, R. (2005). Progress in the synthesis of nanocrystalline BaTiO3 powders for MLCC. International Journal of Applied Ceramic Technology, 2(1), 1-14.

Pugh S. F. :The London, Edinburgh, and Dublin Philosphical Magazine and journal of science, 45 (367), 823-843, (1954).

Raveau, B., Maignan, A., Martin, C., & Hervieu, M. (1998). Colossal magnetoresistance manganite perovskites: relations between crystal chemistry and properties. Chemistry of materials, 10(10), 2641-2652.

Reshak, A. H. (2016). Transport properties of the n-type SrTiO 3/LaAlO 3 interface. RSC Advances, 6(95), 92887-92895.

Sarwan, M., Shukla, P., & Singh, S. (2020). Structural stability, electronic and elastic properties of cubic RbTaO3 perovskite oxide. In AIP Conference Proceedings (Vol. 2265, No. 1, p. 030341). AIP Publishing LLC.

Schneemeyer, L. F., Waszczak, J. V., Zahorak, S. M., van Dover, R. B., & Siegrist, T. (1987). Superconductivity in rare earth cuprate perovskites. Materials research bulletin, 22(11), 1467-1473.

Sin'ko G. V. and Smirnow N. A. (2002). J. Phys. Condens. Matter 14, 6989.

Tahiri, O., Kassou, S., & Mrabet, R. (2018). First principles calculations of electronic and optical properties for mixed perovskites: Ba (1-x) Ca (x) TiO 3 and Ba (1-x) Sr (x) TiO 3 (x= 0.4, 0.6). Materials and Devices, 3, 2004-2018.

Tian, Z., Wang, X., Shu, L., Wang, T., Song, T. H., Gui, Z., & Li, L. (2009). Preparation of nano BaTiO3-based ceramics for multilayer ceramic capacitor application by chemical coating method. Journal of the American Ceramic Society, 92(4), 830-833.

Tsurumi, T., Adachi, H., Kakemoto, H., Wada, S., Mizuno, Y., Chazono, H., & Kishi, H. (2002). Dielectric properties of BaTiO3-based ceramics under high electric field. Japanese journal of applied physics, 41(11S), 6929.

Wu, Z., Hao, X., Liu, X. and Meng, J. (2007). Phys. Rev. B. 75(5), 054115.